acta physica slovaca vol. 54 No. 3, 251 – 262 **June 2004**

LASER ACTION ON MAGNESIUM AND ALUMINIUM TARGETS

V. Henč-Bartolić[1,2], H.-J. Kunze[3], E. Kovačević[3], M. Stubičar[4]
[2] *University of Zagreb,Faculty of Electrical Engineering and Computing Unska 3, 10000 Zagreb, Croatia*
[3] *Ruhr-University of Bochum, Institut für Experimantalphysik V und II Universitätsstr. 150, 44780, Gremany*
[4] *University of Zagreb, Faculty of Science, Bijenička 32, 10002 Zagreb, Croatia*

Received 1 October 2003, accepted 29 January 2004

The beam of a ruby laser was focused onto two targets, $_{12}$Mg and $_{13}$Al, the irradiance being 140 GW/cm^2. In both cases similar processes developed. Time resolved spectra in the region 9-23 nm showed highly ionized atoms. The electron temperature (about 50 eV) and the ion velocities (about 10^6cm s $^{-1}$) were investigated. Due to plasma explosion, deep craters with radial jetting are shown on the target surfaces. Ripples around the craters are explained by spreading of sound waves, laterally deposited plasmas were mixed with expanding target particles.

PACS: 52.50.Jm, 61.80.Ba

1 Introduction

In this work we focused on the spectroscopic study in the soft x-ray region of plasma plumes produced from two targets of elements neighbouring in atomic number, i.e. of magnesium (12) and aluminium (13), using a nanosecond laser pulses. Also the effect of the laser on the surfaces of both solid targets was studied.

Magnesium and aluminium have been chosen because of their similar structural properties (Table 1). Both targets are lightweight metals with nearly equal low melting points. Specific heats and heats of fusion are also similar. However, density at 293 K, thermal conductivity, electrical conductivity and boiling point are about twice higher for aluminium than for magnesium.

2 Experimental set-up

Plasmas were produced by a ruby laser (KORAD K1 laser and K 1500 amplifier) working at the wavelength 694.3 nm with a pulse energy of 5 J, a pulse duration of about 18 ns, i.e. with light fluxes of up to 150 GW/cm^2. In the vacuum chamber (10^{-3} Pa) the laser beam was focused perpendicularly onto the flat Mg or Al target by a plane-convex lens of a focal length f =

[1] E-mail address: visnja.henc@fer.hr

Tab. 1. Properties of targets [1].

	Magnesium	**Aluminium**
Atomic number	12	13
Atomic mass	24.3050	26.981539
1^{st} ionization potential	7.65 eV	5.99 eV
2^{nd} ionization potential	15.04 eV	18.83 eV
3^{rd} ionization potential	80.14 eV	28.45 eV
4^{th} ionization potential	109.25 eV	119.99 eV
Melting point	648.8 ^{o}C	660.4^{o}C
Boiling point	1090^{o}C	2519 ^{o}C
Specific heat	1.02 J/gK	0.90 J/gK
Heat of fusion	8.954 kJ/mol	10.790 kJ/mol
Heat of vaporization	127.40 kJ/mol	293.40 kJ/mol
Thermal conductivity(298K)	1.56 W/cmK	2.37 W/cmK
Density (293K)	1.738 g/cm ^{3}	2.702 g/cm ^{3}
Hardness	2 Mohs	2.75 Mohs

300 mm. The diameter of the focal spot was 0.5 mm. The Mg-/Al- target was situated at the end of a smooth glassy carbon plate (Fig. 1) on a moveable target holder, which allowed that each laser shot was directed onto a fresh spot.

The plasma cloud generated from the target was observed side-on with a VUV flat-field spectrograph equipped with a gateable microchanel-plate and CCD camera. More details can be found in the literature, e.g. in Ref. [2].

3 Spectral analysis

Time-resolved spectra of the plasma radiation were observed in the soft x-ray region from 9 nm to 23 nm with a time resolution of about 10 ns, and variable time delay after the pulse. Spectral images were taken from about 0.7 ± 0.5 mm from the target surface. The instrumental FWHM was about 0.1 nm and line-profiles were not resolvable. In the observed spectral region Mg spectra showed ion lines up to Mg VII with the most intensive emission from Mg IV and Mg V. The most intensive emission in the case of Al plasmas originated from Al IV and Al V ions, with the highest observed ionization stage being Al XI.

Figure 2 presents a Mg spectrum at time $\Delta t = 32$ ns. The Δt is the time interval between the maximum of laser irradiation and the time when the spectra were recorded. Figure 3 presents an Al spectrum at the time $\Delta t = 15$ ns. From recorded spectra it was observed in both cases that the emission (line) intensity of highly ionized atoms decreased, but the intensity from less ionized atoms increased in time. This becomes obvious if we observe the time dependence of intensities of some specific lines, for example from Mg V, Mg IV and Mg III (Table 2), as shown on Fig. 4. Harilal, Bindhu and Kunze [4] investigated in detail space and time-resolved the

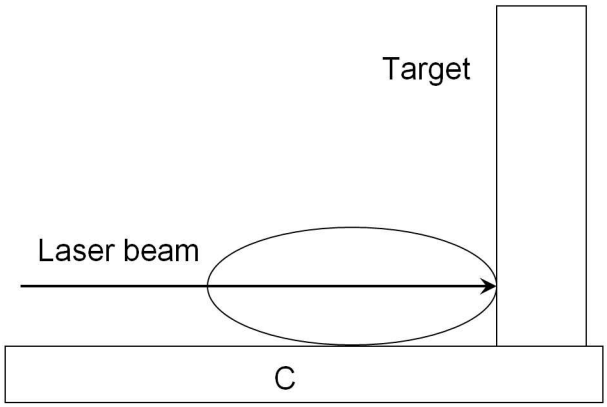

Fig. 1. Target position.

soft x-ray emission from laser-produced magnesium plasmas in the spectral region 3-12 nm at irradiances of $(1.2 - 2.8)\times 10^{11}$ W/cm^2. Assuming local thermal equilibrium (LTE) as a coarse approximation, the electron temperature of the plasmas was estimated to about $\sim 40 \pm 10$ eV at a distance of 5 mm from the target surface. Similar results were obtained for aluminium in Ref. [5]. Following their procedure we also could derive a temperature near the target surfaces of ~ 50 eV for both samples, Mg and Al.

Because our measurements were done in the high irradiance regime, i.e. the light flux exceeded 10 GW cm^{-2} , the particle velocity was estimated using the model of self-regulating plasmas developed by Caruso and Gratton [6]:

$$\nu = \sqrt{\frac{(1+Z)RT}{M}}\,, \tag{1}$$

where Z is the average ion charge (~ 4), R is the gas constant, T is the electron temperature in K, and M is the molar mass (magnesium 0.024306 kg/mol and aluminium 0.026982 kg/mol). The

Tab. 2. The parameters of spectral lines [3].

	λ/nm	E_H/eV	E_B/eV	Transition	J
Mg V	11.43	0.22	108.70	$2p^4\,^3P - 3d^1\,^3P^o$	1 – 2
	11.48	0.00	108.01	$2p^4\,^3P$ - $3d^1\,^3D^0$	2 – 1,2,3
	11.50	0.22	108.01	$2p^4\,^3P$ - $3d^1\,^3D^0$	1 – 1,2
Mg IV	18.01	0.00	68.85	$2p^5\,^2P^0 - 3s\,^2P$	3/2 –1/2
	18.06	0.00	68.64	$2p^5\,^2P^0 - 3s\,^2P$	3/2 - 3/2
	18.08	0.28	68.85	$2p^5\,^2P^0 - 3s\,^2P$	1/2 - 1/2
Mg III	18.65	0.00	66.47	$2p^6\,^1S - 3d^1[\,1\,1/2]^0$	0 – 1
	18.72	0.00	65.83	$2p^6\,^1S - 3d^1[\,1\,1/2]^0$	0 – 1
	18.85	0.00	65.76	$2p^6\,^1S - 3d^1[\,1\,1/2]^0$	0 – 1

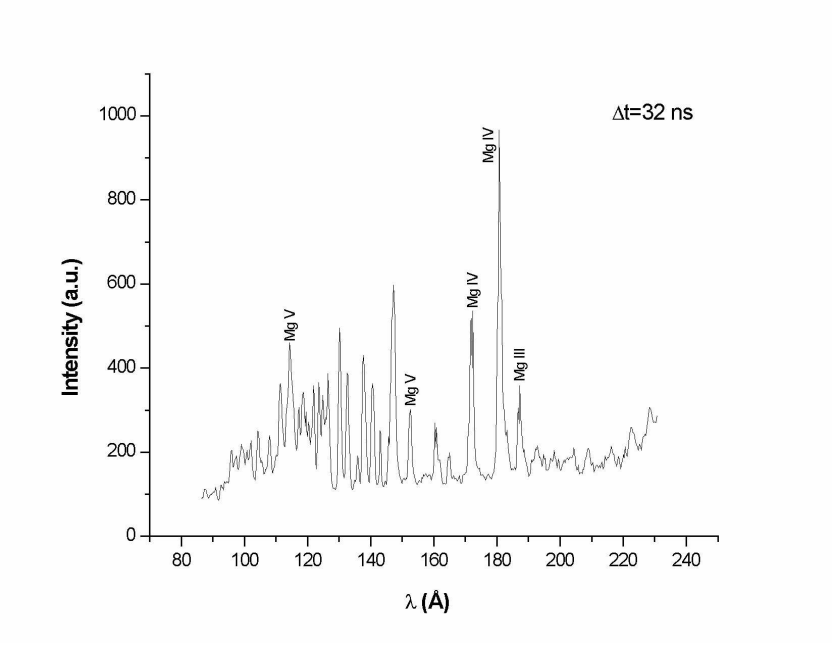

Fig. 2. Soft x-ray spectrum of an magnesium plasma: 32 ns after the maximum of the laser pulse.

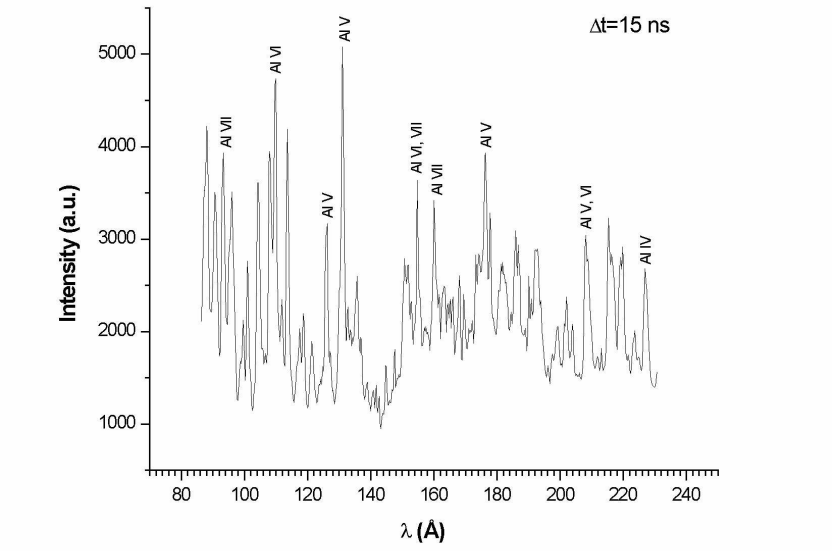

Fig. 3. Soft x-ray spectrum of an aluminium plasma 15 ns after the maximum of the laser pulse.

velocities were $\nu_{\mathrm{Mg}} \sim 3.1 \times 10^6$ cm/s and $\nu_{\mathrm{Al}} \sim 3.0 \times 10^6$ cm/s. According to the theoretical prediction from above Eq. (1), the velocities of the atoms should depend on the inverse square root of its molar mass. Because of the almost identical molar mass of Mg and Al ($M_{\mathrm{Al}} : M_{\mathrm{Mg}} \approx 1.11$), we can take the same velocity for both cases, i.e. about 3×10^6 cm/s .

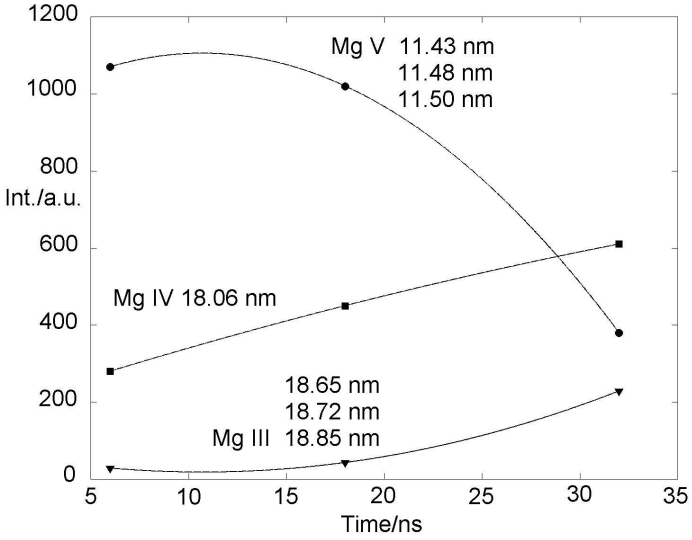

Fig. 4. Temporal evolution of the emission of some specific Mg- ionisation stages.

4 Surface observations

4.1 Magnesium

The surface of the Mg target was analysed with a light (metalographic)- and a scanning electron-microscope. The burn size mark on the target after one shot is about 4.7 mm^2 including the crater and ripples (Fig. 5). The crater has a surface area of 1.1 mm^2 and is of elliptical shape. The depth of the central crater is about 25 μm what can be described as a "deep" crater. This could be expected due to the low melting point, low boiling point and density of magnesium. Employing the light microscope Fig. 6 shows the crater edge with a peripheral zone of radial jetting. This is explained by the regime of plasma explosion [7]. The edge of a second small plasma crater (Fig. 7) is visible a few μm above the bottom. A melted frozen surface with not-ejected droplets is seen at the bottom of the crater (Fig. 8).

The first main crater is surrounded by ripples (Fig. 5 and 9). This can be explained in the following way: It is known that the surface tension of liquids decreases with temperature, and liquid tends to be pulled away from hotter towards cooler regions (Maragoni effect) (see e.g. Ref. [8]. We may assume that pulsed melting of the Mg target causes on abrupt local increase in density, which acts as a strong source for acoustic waves. Waves frozen-in after irradiation

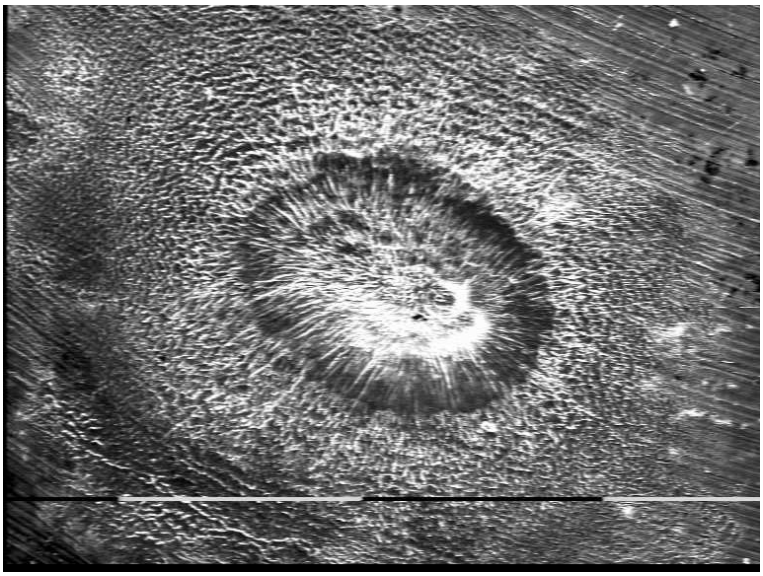

Fig. 5. SEM micrograph of the burn mark on the Mg-target surface (crater and ripples). The scale in the image corresponds to 1 mm.

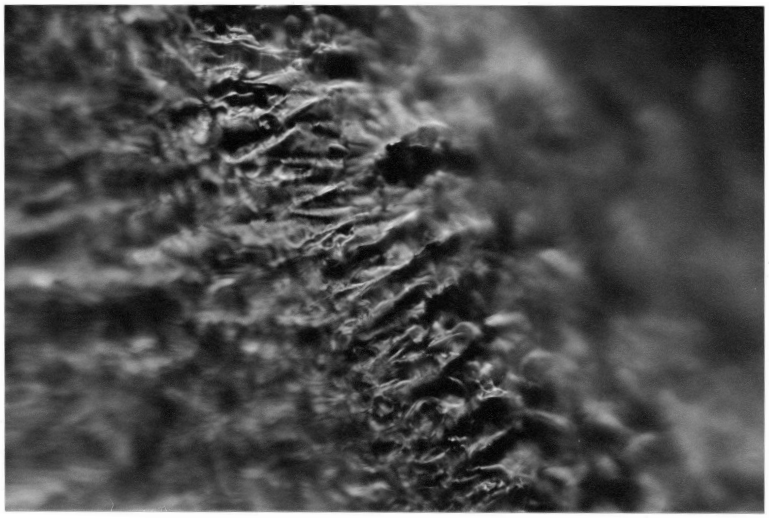

Fig. 6. Optical micrograph of the first, main Mg-crater edge (detail).

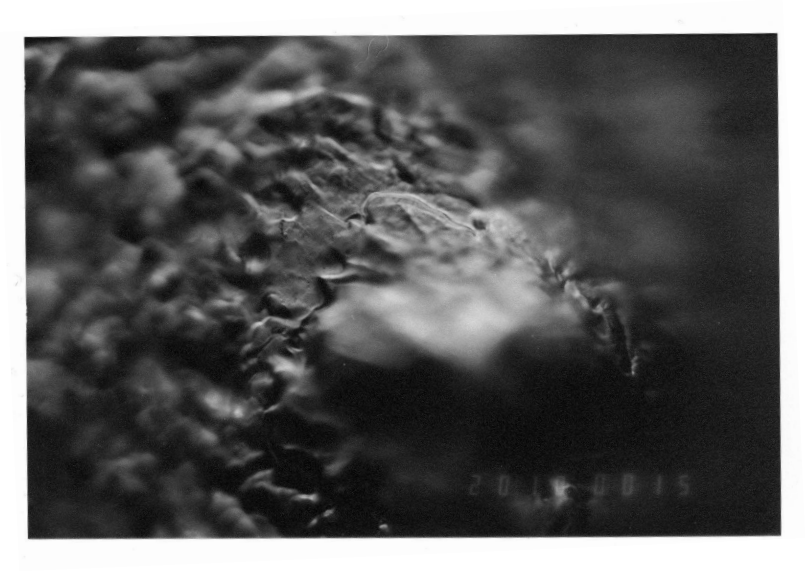

Fig. 7. Optical micrograph of the second Mg-crater edge (detail).

Fig. 8. Optical micrograph of the damage at the bottom.

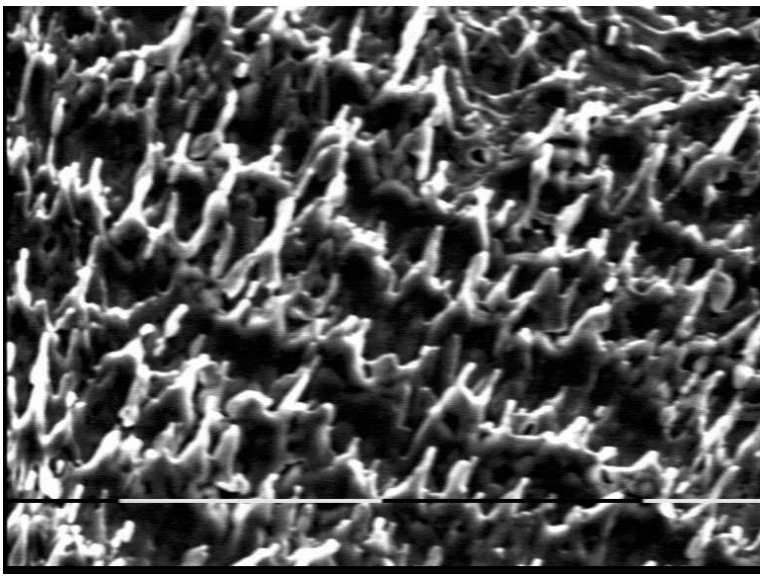

Fig. 9. SEM micrograph of ripples around the main Mg-crater. The scale in the image corresponds to 0.1 mm.

have been correlated to surface ripples with wavelengths in the micrometer range [8]. In the case of the Mg-target, (Fig. 9) the wavelength is about 40 ± 5 μm. We verified this value with a simple calculation. Taking the surface wave velocity to be 3×10^5 cm/s and the frequency to be the inverse of the laser pulse width [9] ($\tau_{\rm laser} = 18$ ns), a wave length of around 60 μm is obtained. It is in reasonable agreement with the observed periodicity. At places where the density of dissolved magnesium was maximal, not-ejected droplets are visible (Fig. 9).

4.2 Aluminium

The surface of the aluminium target was also analysed with the light (metalographic)- and scanning electron- microscope. Contrary to the magnesium target, ripples around the crater were not clearly observed in this case (Fig. 10). The crater had a surface area of about 0.5 mm^2 and an elliptical shape. The throat of the crater (central part of the crater) was ~ 25 μm deep and narrow. On the wall of the throat, ripples are observed with a wavelength of about 6 μm (Fig. 11).

5 Observations of plasma-deposited layers

When we analysed the smooth glassy carbon plate, that was situated at the end of the Mg-/Al-target plate (as shown in Fig. 1), employing also the light or electron microscope the traces of deposited plasmas were visible i.e. a side projection of the plasma plume. Figure 12 is a micrograph which shows the shape of the magnesium plasma cloud. Besides of a thin layer of deposited Mg-plasma, also frozen melt-ejected droplets are visible. The aluminium deposit shows the same characteristics. The deposited clouds are non-homogenous and fan-shaped. The

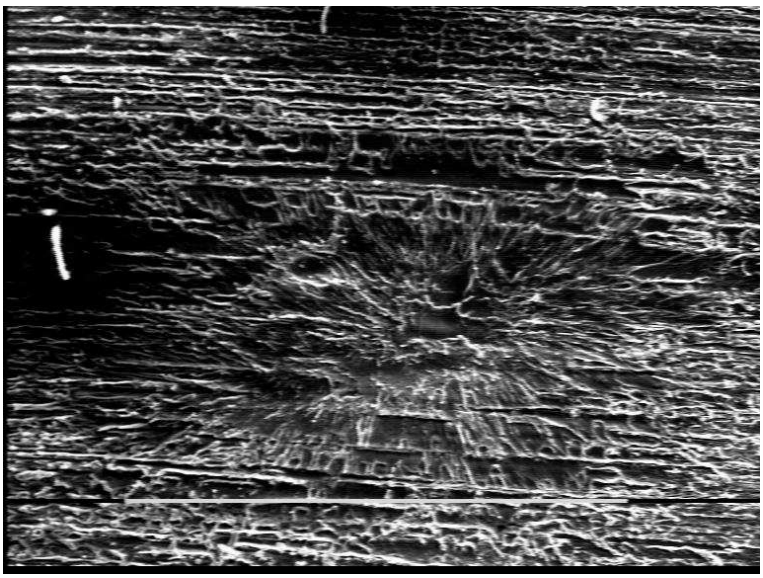

Fig. 10. SEM micrograph of the burn mark on the Al-target surface. The scale in the image corresponds to 1 mm.

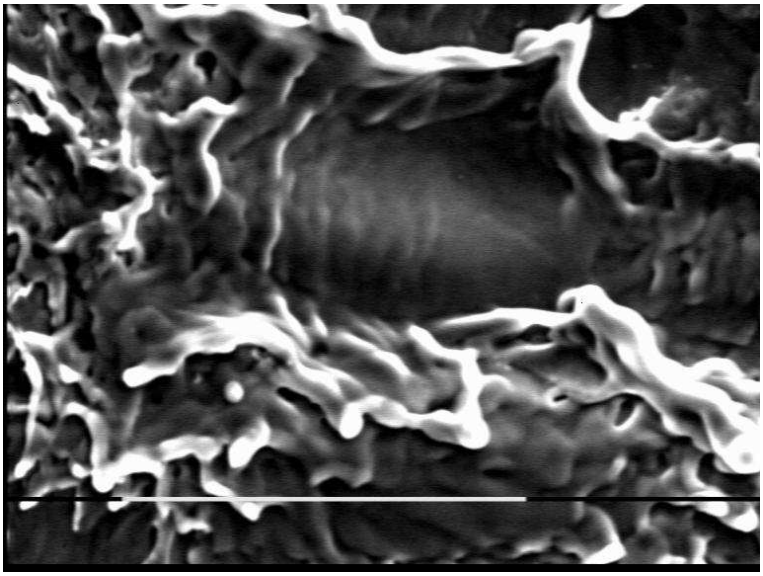

Fig. 11. SEM micrograph of the central part of the Al- target surface. The scale in the image corresponds to 0.1 mm.

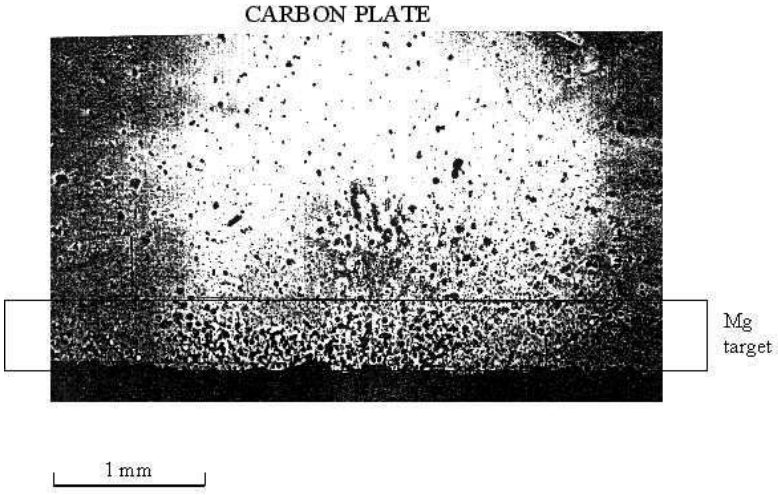

Fig. 12. Mg-plasma cloud shape-SEM micrograph of the surface of the glassy carbon plate.

thickest Mg/Al plasma layer was recorded in the region of the original laser focal spot diameter (0.5 mm) and was spread in perpendicular direction from the target up to $\sim$ 1 mm. The length of the total deposit is $\sim$ 2.5 cm and its width is $\sim$ 3 cm. The diameters of the frozen droplets vary from 5 to 30 μm. Sometimes droplets stick together in an irregular shape. The plasma deposit Mg/Al-contours can be explained by strongly non-linear Rayleigh-Taylor (RT) plasma instabilities. We can compare this observation with previous works [7,11,12].

6 Discussion

A spectral study was done in the soft x-ray region with the intention to investigate the dynamics of the highly charged ions in laser-produced magnesium and aluminium plasmas. We assume that recombination processes can explain the observed intensity decrease of lines from higher ionized atoms and the intensity increase of lines from less ionized atoms (Fig. 4). Time resolved measurements show that ions have a high expansion velocity corresponding to a kinetic energy of $\sim$ 113 eV for magnesium and of $\sim$ 125 eV for aluminium ions, respectively.

The processes which are reflected on the walls of the crater throats (Figs. 7, 8 and 11) are most likely provoked by an oscillating absorption coefficient of the plasma. We are going to explain it.

The mechanism responsible for plasma absorption at the high laser irradiation level (140 GW cm^{-2}) is inverse bremsstrahlung [4]. The inverse absorption length or absorption coefficient is given by [4,10]:

$$\alpha \approx 1.27 \times 10^{-46} \lambda^3 Z^2 n_e n_i T_e^{-1/2} \left[1 - \exp\left(-\frac{h\nu}{kT_e}\right)\right], \quad (2)$$

where λ is the wavelength of the laser photons in nm, kT_e is the electron temperature in eV, $h\nu$

is the laser photon energy in eV, Z is the average ionic charge and n_i and n_e are the ion and electron densities in cm^{-3}, respectively. Due to the high temperature (50 eV) the exponential term in Eq. (2) $\Rightarrow 1$ (becomes unity) at the laser wavelength (694.3 nm). Hence the absorption coefficient simplifies to

$$\alpha = C\lambda^2 Z^2 n_e n_i T_e^{-3/2}, \tag{3}$$

where C is a constant.

This yields $\alpha \approx 0.1$ cm^{-1} for our experiments assuming an electron density of 10^{19} cm^{-3} [4]. The plasma absorption of the incident laser radiation is high only near the target surface, where the density of the ionized species is also high and a self-regulating regime is restored [11]. Singh, Holland and Narayan in [13] give the next conclusion: "If the absorption of the laser light by the plasma becomes high, the evaporation of species from the target becomes less, thus decreasing the density of the ionized species and, consequently, the absorption of the laser beam. If instead absorption by the plasma is less, the process is reversed with similar results". In our experiments the pulse duration of the laser used is long (~ 18 ns), and we therefore assume that the absorption coefficient oscillates in magnitude during laser irradiation.

Reflection of incident laser photons does not take place, because the plasma frequency is smaller than the laser frequency [4,8].

Finally, we have to point out, that at high laser irradiation droplets are ejected from the targets, either by boiling or by evaporation recoil (Fig. 12). Also, ripples around the main Mg-crater were observed.

7 Conclusion

In this paper we report on the study of the action of a ruby laser pulse on magnesium and aluminium targets. Processes developed at the two different targets were similar because of their similar structural properties.

In agreement with an earlier study [4], soft x-ray photons and high expansion velocities of ions were observed in both (Mg/Al) cases at high laser irradiation.

On the peripheral zones of the Mg-/Al-crater edges radial jetting was observed. It is obvious that a plasma explosion developed.

It is known, that at irradiances well above the melt threshold uniform melting occurs, and lateral variations of the melt temperature become the relevant force for imprinting patterns in the material [8]. On the Al surface the ripples are not regular and not clearly observed, and the throat of the aluminium crater is narrower than that of the crater in magnesium. We relate all this to the fact that the boiling point is 2.3 times higher for aluminium than for magnesium.

The traces of deposited plasma on side projections of the plasma plume were mixed with solidified ejected droplets from the target craters.

Table 1 shows that the thermal conductivities are different for the two investigated metals. We conclude, this difference is not significant at our conditions, the reason being that the conductivity of metals above room temperature and especially after the melting point show a drop in its magnitude [8].

Our measurements provide information for further investigations in the field of laser induced plasmas and laser ablation of target surfaces in the high irradiation regime.

Acknowledgement: The authors gratefully acknowledge the help of Mr. W. Oswaldand Mrs. D. Petrinovič. The work was supported by the Institute of Experimental Physics 5^{th}, Ruhr-University Bochum, Germany and Croatian Ministry of Science and Technology.

References

[1] *http://www.vcs.ethz.ch/chemglobe/ptoe/_/12t.html*

[2] Z. Andreič, L. Aschke, H.-J, Kunze: *J. Phys. D.: Appl. Phys.* **31** (1998) 1487

[3] A.R. Striganov, N.S. Sventitskii: *Tables of Spectral Lines of Neutral and Ionized Atoms*, New York, IFI/Plenum 1968

[4] S.S. Harilal, C.V. Bindhu, H.-J. Kunze: *J. Phys. D.: Appl. Phys.* **34** (2001) 560

[5] L. Aschke: *Diplomarbeit*, Bochum: EP V, Ruhr Universiät Bochum 1995

[6] A. Caruso, R. Gratton: *Plasma Physics* **10** (1968) 867

[7] S. Lugomer: *Laser-Matter Interaction*, Profil, Zagreb 2001

[8] M. von Allmen, A. Blatter: *A Laser-Beam Interaction with Materials*, Second Edition, Springer, Berlin 1995

[9] G. Gorodetsky, J. Kanicki, T. Kazyaka, R.L. Melcher: *Appl. Phys. Lett.* **46** (1984) 547

[10] Y.B. Zel'dovich, Y.P. Raizer: *Physics of Shock Waves and High Temperature Hydrodynamic Phenomena*, Academic, New York 1966

[11] E. Kovačević, V. Henč-Bartolić, H.-J. Kunze: *Conf. Procedings, ICECom 2001, 16^{th} Int. Conf. on Appl. Electromagnetics and Comunications.* (Eds. KoREMA) 2001, p. 194

[12] V. Henč-Bartolić, E. Kovačević, H.-J. Kunze, M. Stubičar: *J. Tech. Phys.* **44** (2003) 153

[13] R.K. Singh, O.W. Holland, J. Narayan: *J. Appl. Phys.* **68** (1990) 233